Soft Matter

Controlling Toughness of Polymer-grafted Nanoparticle Composites for Impact Mitigation

Journal:	*Soft Matter*
Manuscript ID	SM-COM-10-2021-001432.R1
Article Type:	Communication
Date Submitted by the Author:	16-Nov-2021
Complete List of Authors:	Chen, Shawn; National Institute of Standards and Technology, Materials Measurement Sciences Division Souna, Amanda; National Institute of Standards and Technology, Materials Science and Engineering Division Stranick, Stephan; National Institute of Standards and Technology, Jhalaria, Mayank; Columbia University Kumar, Sanat; Columbia University, Soles, Christopher; National Institute of Standards and Technology, Materials Science and Engineering Division Chan, Edwin; NIST, Materials Science and Engineering Division

Soft Matter

ARTICLE TYPE

Cite this: DOI: 00.0000/xxxxxxxxxx

Controlling Toughness of Polymer-grafted Nanoparticle Composites for Impact Mitigation

Shawn H. Chen,[a] Amanda J. Souna,[b] Stephan J. Stranick,[a], Mayank Jhalaria,[c] Sanat K. Kumar,[c] Christopher L. Soles,[b] and Edwin P. Chan[b*]

Received Date
Accepted Date

DOI: 00.0000/xxxxxxxxxx

Toughness in an entangled polymer network is typically controlled by the number of load-bearing topological constraints per unit volume. In this work, we demonstrate a new paradigm for controlling toughness at high deformation rates in a polymer-grafted nanoparticle composite system where the entanglement density increases with the molecular mass of the graft. An unexpected peak in the toughness is observed right before the system reaches full entanglement that cannot be described solely through entanglement concepts alone. Quasi-elastic neutron scattering reveals enhanced segmental fluctuations of the grafts on the picosecond time scale, which propagate out to nanoparticle fluctuations on the time scale 100s of seconds as evidenced by X-ray photon correlation spectroscopy. This surprising multi-scale dissipation process suggests a nanoparticle jamming-unjamming transition. The realization that segmental dynamics can be coupled with the entanglement concept for enhanced toughness at high rates of deformation is a novel insight with relevance to the design of composite materials.

When a melt of short amorphous polymers such as polystyrene (PS) is mechanically deformed, the chains are readily pulled apart from their neighbors through frictional sliding. This failure mechanism is known as "chain pullout". Chains longer than a threshold molecular mass (M_c), on the other hand, participate in a topological network which appears analogous to a chemically cross-linked rubber network in an instantaneous snapshot. While frictional sliding of the chains in this network can occur, the chains must respect the topological constraints imposed by these entanglement points – the chains can thus reptate and relax stress without causing covalent bond rupture. At sufficiently high molecular mass, however, the viscous drag on an individual strand, which is obtained by integrating the forces along the length of the chain, can exceed the strength of the covalent bonds. At this point the chain will rupture via chain scission. This mechanism is especially prominent in polymers like PS where the molecular mass between the junctions is large and fewer opportunities are present to transfer the load between neighboring chains through the topological entanglements. Both chain disentanglement and scission reduce the number of entanglements in the network and initiate yield or failure. The particular failure mechanism that a polymer undergoes depends on its overall molecular mass, the number of entanglements per chain, the monomeric friction coefficient for chain sliding, as well as extrinsic factors such as deformation rate, temperature, and the scale of the fracture test.

Wool's rigidity percolation model has proven effective at describing the interplay of these three processes under quasi-static testing rates, where chain relaxation times (τ_f) are much shorter than deformation times (t_p).[1–3] As shown in **Figure 1a**, the fracture energy (G_c) of PS as a function of molecular mass (M), with $M_c \approx 30$ kg/mol, can be cleanly separated into three regions:

$$G_c \approx \begin{cases} M, & \text{segment pull-out } (M \le M_c) \\ \left(\sqrt{\frac{M}{M_c}} - 1\right)^2, & \text{disentanglement } (M_c < M \le 8M_c) \\ 1 - \frac{M_c}{M}, & \text{chain scission } (M > 8M_c) \end{cases} \quad (1)$$

While much of our understanding of the mechanisms of polymer fracture are based on quasi-static tests, many real world applications involve impulsive and nonequilibrium processes with extremely high rates of deformation where the mechanisms can be quite different. Laser-induced Projectile Impact Testing (LIPIT) enables one to study the fracture of materials at high deformation rates via microballistic fracture tests at impact velocities up to 1 km/s.[2,4–8] Several studies now document unusual or unexpected deformation processes in polymer films under LIPIT testing. To illustrate this point, we present previously published LIPIT data for PS films in **Figure 1b** that corresponds to the condition of $t_p \ll \tau_f$. Our modeling of the data using the rigidity percolation model confirms the chain disentanglement mechanism is no longer ac-

[a] Materials Measurement Sciences Division, National Institute of Standards and Technology, 100 Bureau Dr, Gaithersburg, MD 20899.
[b] Materials Science and Engineering Division, National Institute of Standards and Technology, 100 Bureau Dr, Gaithersburg, MD 20899. E-mail: edwin.chan@nist.gov
[c] Department of Chemical Engineering, Columbia University, 801 SW Mudd, New York, NY 10027.

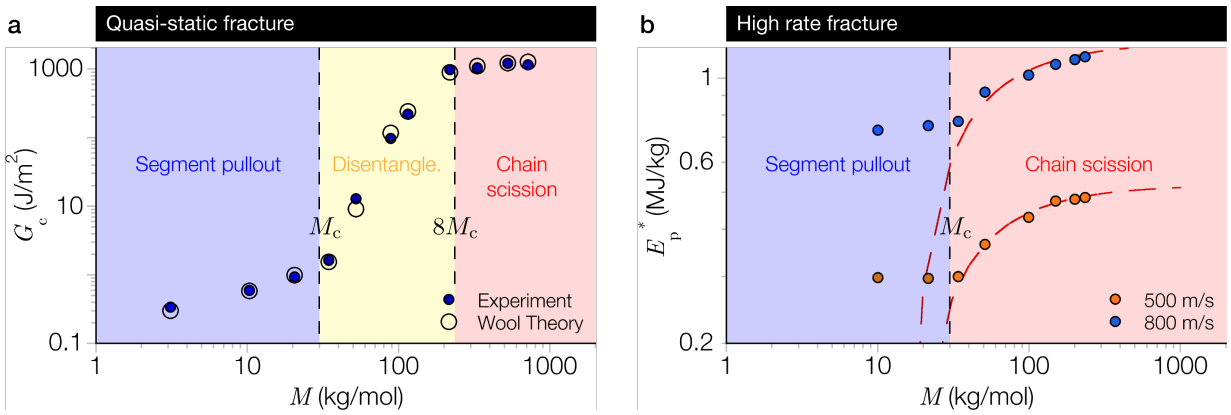

Fig. 1 The molecular mass and deformation rate-dependent fracture mechanisms for polystyrene (PS) homopolymer. a) Fracture energy (G_c) versus molecular mass (M) of PS under quasi-static testing demonstrating that the predicted values from the Wool Theory are in excellent agreement with the experimentally measured values for molecular mass ranging from well below the critical molecular mass for entanglement (M_c) to well above M_c. The three fracture mechanisms include segment pullout ($M \leq M_c$), disentanglement ($M_c < M \leq 8M_c$) and chain scission ($M > 8M_c$). Data reproduced from Ref[1]. b) The high rate fracture behavior, as measured using a microballistic puncture test, for PS thin films is significantly different over a similar range of molecular mass. Data reproduced from Ref[2]. The red curve is based on the rigidity percolation model for chain scission.

tive at the high rate of impact achieved by LIPIT; rather, chain scission dominates with increasing strain rates.[1,9] This is evident in **Figure 1b** where the apparent fracture energies (E_p^*) obtained from LIPIT microballistic fracture test of PS films[2] are plotted as a function of molecular mass. It is also striking that the rigidity percolation model is still able to parameterize the transition between these two deformation modes, even under nonequilibrium loading conditions such as LIPIT.

There is considerable interest in being able to increase the impact resistance of soft polymeric materials. An extremely promising materials platform is polymer-grafted nanoparticles (PGNs), which is a composite composed of polymers covalently grafted onto inorganic nanoparticles (NP). These designer nanocomposites eliminate the undesirable aggregation of NPs commonly seen in conventional polymer nanocomposites while enhancing the overall electrical, mechanical, optical, thermal, and transport properties.[8,10–22] In this work, we study the high rate fracture behavior of films made with polymethylacrylate (PMA) grafted SiO_2 nanoparticles using LIPIT as a means to quantify the apparent toughness at high deformation rates ($\sim 10^5$ s^{-1}).[23] In addition to the entanglement driven toughening mechanisms discussed above, we show that these materials possess a new handle, the segmental relaxation times, that allows us to significantly increase the materials' high-rate impact toughness especially where the brushes transition through their entanglement molecular mass. These results also manifest themselves in the NP dynamics which show a sharp minimum, likely reflecting the transition from a colloid-dominated to an entangled polymer-dominated regime. These results assert the polymer systems have two variables, the entanglement density and relaxation times, that can control toughness – under special circumstances, as in the case of the PGNs, we can separately manipulate these with unexpectedly favorable consequences on ultimate properties.

Details of the LIPIT experimental procedure, sample preparation and characterization are found in the SI and prior publications.[16,24] We first compare the impact (v_i) and residual velocities (v_r) of the impacting microprojectile (**Figure 2a**). As expected, we find that v_r increases with v_i across all of the materials. The post-fracture surfaces of the PGN films (**Figure 2b**) exhibit distinct differences in the fracture behavior of the films as a function of M. At low M (< 55 kg/mol), the films fail with large extended cracks characteristic of brittle fracture. With increasing M (> 55 kg/mol), the fracture becomes more confined around the point of impact, and we find circular exit holes with diameter approximately equal to the impacting microprojectiles (≈ 25 μm). We use this data to quantify the specific puncture energy, $E_p^* = m_p(v_i^2 - v_r^2)/2m_f$, which is the kinetic energy loss of the microprojectile of mass m_p normalized by the mass of the plug of the film (m_f) that interacted with the microprojectile.[7] The key result of our work (**Figure 2c**) is that E_p^* does not increase monotonically with molecular mass of the PMA as observed in previous LIPIT studies.[6,7,22,23] E_p^* instead reaches a maximum at $M \approx 96$ kg/mol, with a value that is $\approx 1.3\times$ greater than the most entangled (184 kg/mol) PGN system. For $M > 96$ kg/mol, E_p^* appears to plateau towards a lower value that is roughly equal to the value for neat PMA (with no NPs) with a molecular mass of 122 kg/mol. Intriguingly, the gas permeation behavior of these PGNs also show an unexpected increase relative to the neat PMA, with an enhancement that is nearly an order of magnitude for $M \approx 96$ kg/mol (**Figure 3c**).[16] Unpublished thermal conductivity data also show a maximum with increasing M at roughly the same molecular mass. These PGNs with chain lengths in the vicinity of this maximum have unusual transport properties that we expect are tied to the origins of the mechanical toughening that are of interest to this work through the dynamics of the polymer grafts, a concept that we will develop below. It is worth noting that evidence of significant adiabatic heating at the site of impact have been reported previously in LIPIT-based projectile impact tests[6–8,25], and we believe that the phenomenon contributes to the local dynamics that underpin the toughening behavior observed.

Before we attempt to understand this unusual result in terms of

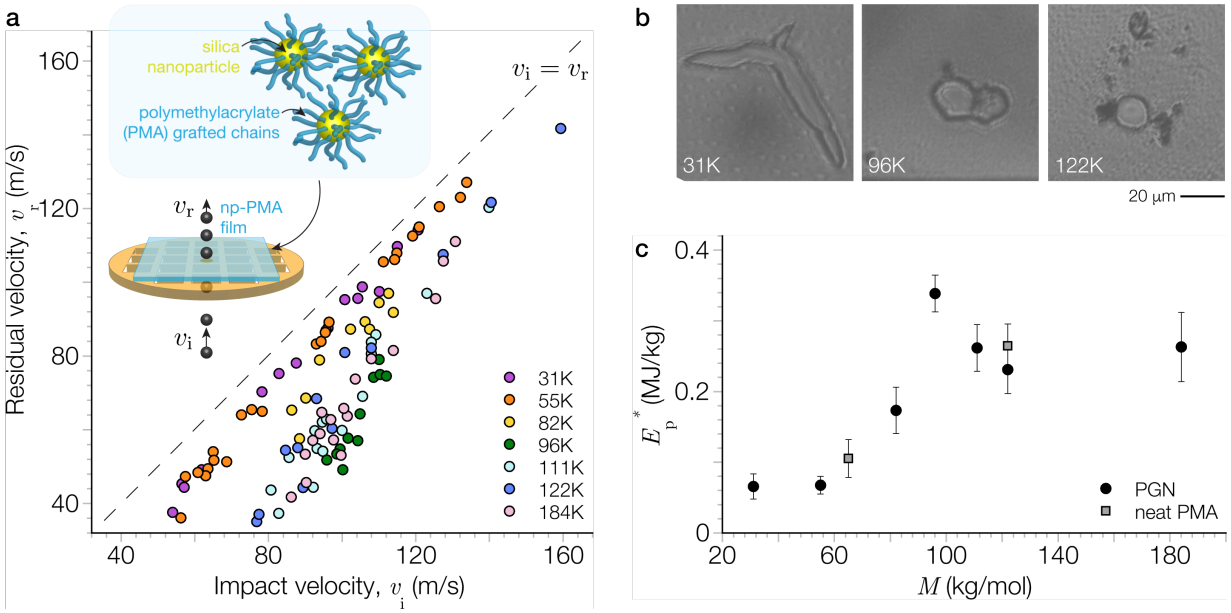

Fig. 2 Laser-induced Projectile Impact Testing (LIPIT) results of the polymer grafted nanoparticle (PGN) films. a) Residual velocity (v_r) versus impact velocity (v_i) as a function of the molecular mass (M) of the polymethacrylate (PMA). The dashed line indicates the maximum v_r or the scenario in which no energy is transferred to the film, $v_r = v_i$. The inset is a schematic of the PMA chains grafted to the silica nanoparticles, and the LIPIT experiment. b) Top-down optical microscopy images of the post-punctured films illustrating the changes in the fracture surface as a function of M. c) Increasing M results in a non-monotonic increase in the specific puncture energy (E_p^*) calculated from the average of at least three separate impact events. Also included are the E_p^* values for 65 kg/mol and 122 kg/mol neat PMA.

dynamics, it is helpful to first consider the structural evolution of the polymer brush in PGN melts as a function of graft length (at fixed grafting density). We use a two-layer PGN model to illustrate the essential physics.[17] For short grafts at intermediate to high grafting density, the chains are stretched close to the surface ("overcrowding") leading to a polymer brush that does not interpenetrate with brushes on adjacent NPs, *i.e.*, a "dry" brush. With increasing distance from the NP surface there is increased area and hence as the graft chain length increases, the chain segments are less constrained and can interpenetrate with segments from adjacent NPs. This interpenetrated region is critical to the overall mechanical properties of the nanocomposite as it enables the formation of chain entanglements and thus provide load-bearing capability. Detailed derivations are provided in the SI for R_{tot} (the net effective radius of the PGN accounting for the NP core volume and that of the polymer segments), x (characterizes the extent of overcrowding), and M_{inter} (the molecular mass of chains in the interpenetrated zone).

We find that the chain segments for all of PGNs investigated here are interdigitated. The number of entanglements per chain is estimated by normalizing M_{inter} by the critical entanglement molecular mass (M_c), and we find that this value increases with the MW of the grafted polymer chains. The quantity of entanglements per chain assumes a value of ≈ 4 near the peak toughness molecular mass (**Figure 3a**). Furthermore, we can identify the transitions between the three distinct fracture mechanisms as a function of the chain segments that can form entanglements. Region I corresponds to no entanglements ($M_{inter} < M_c$); while none of the samples in this work fall within this region, we expect the fracture toughness in region I to be exceedingly small. In region II, the interpenetrated chain segments exceed the critical threshold for entanglement formation ($M_{inter} > M_c$), and as a result E_p^* begins to rise with increasing M. The orange dotted curve estimates the contribution of chain disentanglement to the overall energy dissipation as a function of interpenetrated chain segment length, $E_p^* \sim \left(\sqrt{M/M_c} - 1\right)^2$. To a first-order approximation, this scaling relationship captures the increase in E_p^* for $1 \leq M_{inter}/M_c < 4$ (**Figure 3a**).

As we have discussed earlier, chain disentanglement is strongly dependent on the rate of deformation and the primary mechanism can transition to chain scission at sufficiently high deformation rates.[1] To identify this transition we compare the time required to disentangle an entangled chain segment (τ_f) with the total time of deformation ($t_p \cong 4 \times 10^{-7}$ s) based on the LIPIT test conditions (**Figure 3b**). Calculations for the time scales can be found in the SI. When $\tau_f/t_p < 1$, the deformation rate is within the threshold at which disentanglement can occur. However, when $\tau_f/t_p \geq 1$, the time scale of the experiment is too fast for chain disentanglement and chain scission is the predominant mechanism. With increasing entanglement density of the PGNs, we can expect a point at which the disentanglement time becomes greater than the deformation rate and chain scission occurs. We find that this transition occurs when $M_{inter} > 80$ kg/mol. We note that the disentanglement to chain scission transition observed here is due to an incommensurability in time scales as opposed to length scales. Since $\tau_f \approx \tau_{RO} \ln(M_{inter}/M_c)$, where τ_{RO} is the Rouse time of the polymer chain,[26] we can identify the transition from disentanglement to chain scission with **Figure 3a**, which occurs at $M_{inter}/M_c \approx 4$ or $M = 96$ kg/mol. Here, the red dashed curve is the scaling relationship ($E_p^* \sim 1 - M_c/M_{inter}$) for chain scission

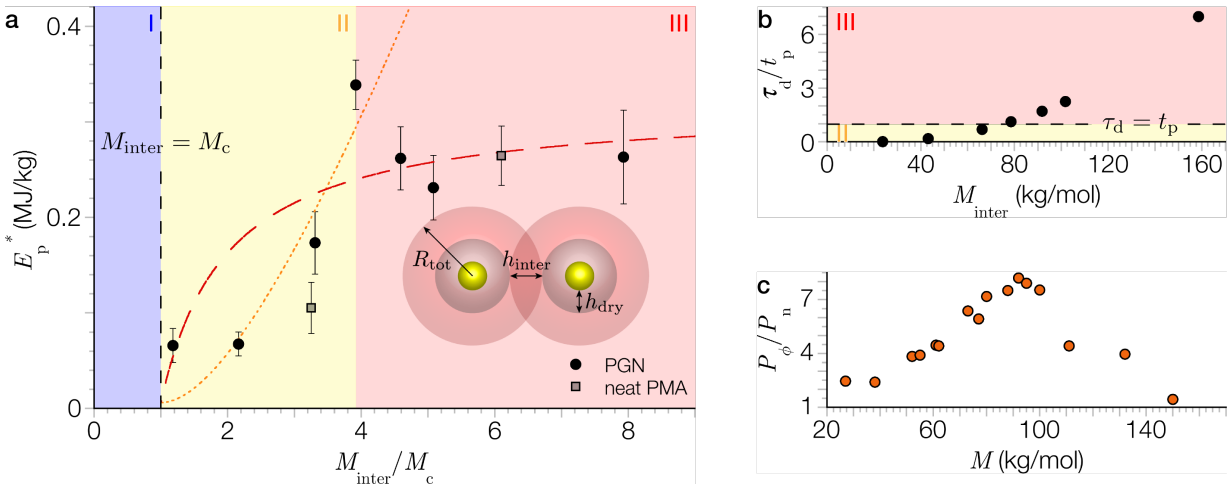

Fig. 3 The fracture mechanisms of the PGN films as a function of M_{inter}. a) The plot of E_p^* versus number of entanglements (M_{inter}/M_c) shows that the energy dissipation results can be categorized into the three distinct molecular mechanisms of deformation. The transition between chain segment pullout (region I) to disentanglement (region II) occurs when $M_{inter} = M_c$. The inset is a schematic of the two-layer PGN model illustrating that the increase in molecular mass of the grafted chains leads to the interpenetration and subsequent entanglement of polymer chain segments between adjacent nanoparticles. b) Plot of dimensionless time ($= \tau_f/t_p$) versus M_{inter}. The transition between disentanglement (Region II) and chain scission (Region III) occurs when $\tau_f = t_p$. c) Plot of the ratio of CO_2 permeability (Data reproduced from Ref.[24]) of the PGN films (P_ϕ) relative to the values for the neat polymer (P_n) as a function M shows that the maximum enhancement in permeability occurs at $M \approx 100$ kg/mol.

(Region III).

While the rigidity percolation model successfully predicts the transition between the different deformation mechanisms, it does not address the enhancement in E_p^* at the crossover between disentanglement and chain scission dominated regimes. As **Figure 3c** shows, this molecular mass (and within its vicinity) corresponds to significant increases in gas permeability and separately thermal transport in these nanocomposites.[24] Such enhancements are not observed in the mechanical properties of PS at either the quasi-static or ballistic rates of deformation (**Figure 1**). To explain this enhancement effect, we turn our attention from the role of entanglements to the ability of the material to dissipate energy. Specifically, we focus on the collective dynamics of the NPs using X-ray photon correlation spectroscopy (XPCS), and the segmental dynamics of the polymer chains using quasi-elastic neutron scattering (QENS). Both reveal that there is a significant enhancement in (multi-scale) dynamics in the vicinity of the toughness maximum. Additionally, we note that adiabatic heating during the LIPIT impact tests raises the temperature of the PGNs above its glass transition thus justifying the consideration of local segmental dynamics.

The details of the XPCS measurements are deferred to the SI. We derive correlation function data corresponding to the silica NP collective structure factor. This data yields a q-dependent relaxation time (**Figure 4a**). We plot the relaxation times at one representative q that corresponds to the structure factor peak as a function of M. The relaxation time, $\langle\tau\rangle$, which characterizes the relaxation of nearest neighbor NPs, clearly shows a minimum around 60 kg/mol (**Figure 4b**). Since the XPCS measurements were conducted at 393 K while the LIPIT measurements were done at room temperature (nearly 100 K lower), we believe that the XPCS results indicate a significant increase in NP dynamics near the toughness maximum. These fluctuations of the NPs occur in the time scale of nominally 100 to 1000 seconds. Previous work has shown that this transition is also presaged in the rheology of these materials[16,19] – the behavior is akin to a jammed solid for lower chain lengths whereas behavior more reminiscent of a polymer melt occurs for larger molecular masses. This transition in XPCS dynamics likely reflects this colloid-to-polymer transition. Starting at large molecular mass and reducing chain length results in lower number of entanglements per chain and hence faster dynamics. Alternatively, the NP relaxation time decreases with increasing chain length for short chains due to lower NP content, resulting in diminishing contribution of the colloidal nature. Where these trends intersect corresponds to the fastest NP relaxations.

Based on these facts, and on previous work,[27,28] we assert that this enhancement in structural dynamics near the toughness maximum is accompanied by a faster local relaxation process, which is important as an energy dissipation mechanism for toughness. To explore this, we preformed quasi-elastic and inelastic neutron scattering (QENS and INS) measurements on the PGNs.

The details of the neutron scattering measurements and their fitting are provided in the SI. Briefly, a narrow Lorentzian captures the quasi-elastic broadening in these spectra with the full-width half-maximum (FWHM) of the fits reported in **Figure 4c**. This reveals a maximum in the FWHM at the same intermediate molecular mass ($M \approx 96$ kg/mol) where the maximum in E_p^* is observed. This quasi-elastic broadening reflects fast relaxations of the PMA chains, and this processes is the fastest when $M \approx 96$ kg/mol. Also shown in **Figure 4c** are the corresponding time constants (τ) for these relaxations which range from approximately 1.9 ps to 2.6 ps. We showed that the activation of these relaxation processes on time scales longer than a few ps are critical for ductility and toughness in polycarbonates.[27,28] The result presented here is important because it indicates that faster

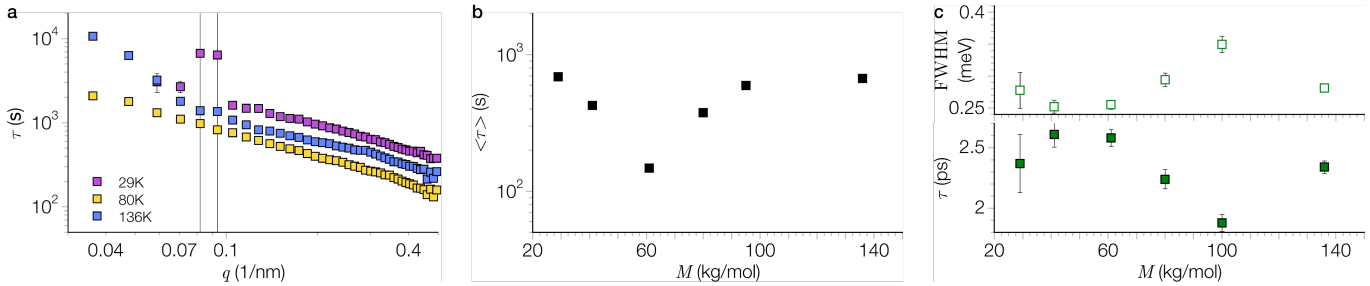

Fig. 4 a) Relaxation time (τ) as a function of q for neat PMA with M = 29 kg/mol, 80 kg/mol, and 136 kg/mol captured from XPCS measurements. b) Mean relaxation time extracted from the results in a) at one representative q ($\langle\tau\rangle$) that corresponds to the structure factor peak as a function of M reveal a minimum around 60 kg/mol. c) Full-width at half-maximum (FWHM) from the QENS measurements versus M of the PGN materials indicating the enhanced dynamics at $M \approx 100$ kg/mol and the corresponding relaxation times (τ).

relaxations are more effective at enhancing toughness. This enhancement in *sub*-ns dynamics is also seen when we compare the change in mean-square displacement ($\langle u^2\rangle$) across the different materials obtained from temperature dependent INS measurements. Previously, we correlated the level of anharmonicity in $\langle u^2\rangle$ with the Izod impact strength across a series of polycarbonate glasses.[27] A measure of this anharmonicity is the "softness" of the effective spring constant (k') obtained from the temperature dependent slope of ($\mathrm{d}\langle u^2\rangle/\mathrm{d}T$). As detailed in the SI, k' also goes through a minimum near $M \approx 96$ kg/mol that is consistent with the peak in E_p^*. The enhanced molecular mobility and relaxation processes on *sub*-nanosecond (INS) and picosecond (QENS) time scales are clearly important for dissipating energy. We note that the time scale for these relaxations are still sufficiently fast compared to the deformation rate encountered in LIPIT making it reasonable that they contribute to energy absorption. The dissipative contribution is separate from the chain entanglement effects discussed previously. In the context of the rigidity percolation model, this enhanced dissipation is probably akin to a reduction of the monomeric friction coefficient, although this connection is yet to be formally established.

The LIPIT results show that polymer entanglements alone do not enhance toughness since the entanglement density increases with molecular mass of the grafted chains. Conversely, nanoparticle jamming alone cannot describe the enhanced toughness since jamming is more pronounced with shorter grafted chains. These results would suggest that the enhancement in toughness seen for the 96 kg/mol system requires synergy of these two mechanisms of energy dissipation. The polymer-dominated response is augmented by a hierarchical relaxation mechanism where the highly localized chain segment retraction is followed by a colloidal relaxation process over a larger length scale as revealed by the XPCS results.[29] XPCS and QENS measurements highlight the enhanced dynamics at this transition, and they point to a correlation between chain dynamics and material toughness. While our results indicate that it would be quite challenging for an existing polymer-based impact mitigating material to be useful over a broad range of deformation rates, this seminal work has begun to explore the remarkable and highly tunable mechanical properties of PGNs. There is vast potential in leveraging this mechanism to design polymeric materials with dynamically tunable molecular response that maximizes impact mitigation performance.

Conflicts of interest

Certain commercial equipment, instruments, or materials are identified in this paper in order to specify the experimental procedure adequately. Such identification is not intended to imply recommendation or endorsement by NIST, nor is it intended to imply that the materials or equipment identified are necessarily the best available for the purpose.

Acknowledgements

The research used resources of the Advanced Photon Source and the Center for Nanoscale Materials, U.S. Department of Energy (DOE) Office of Science User Facilities operated for the DOE Office of Science by Argonne National Laboratory under Contract No. DE-AC02-06CH11357. Financial support for this work at Columbia (MJ, SKK) was provided by the Department of Energy under grant DE-SC0021272.

Access to HFBS was provided by the Center for High Resolution Neutron Scattering, a partnership between the National Institute of Standards and Technology and the National Science Foundation under Agreement No. DMR-1508249.

SHC acknowledges financial support from the NIST National Research Council Postdoctoral Research Associateship. This work is a contribution of NIST, an agency of the U.S. Government, and not subject to U.S. copyright.

Notes and references

1 R. P. Wool, *J. Polym. Sci. B Polym. Phys.*, 2005, **43**, 168–183.
2 W. Xie and J.-H. Lee, *Macromolecules*, 2020, **53**, 1701–1705.
3 R. P. Wool, D. M. Bailey and A. D. Friend, *J. Adhes. Sci. Technol.*, 1996, **10**, 305–325.
4 J.-H. Lee, D. Veysset, J. P. Singer, M. Retsch, G. Saini, T. Pezeril, K. A. Nelson and E. L. Thomas, *Nat Commun*, 2012, **3**, 1164.
5 D. Veysset, A. J. Hsieh, S. E. Kooi and K. A. Nelson, *Polymer*, 2017, **123**, 30–38.
6 J. Hyon, O. Lawal, O. Fried, R. Thevamaran, S. Yazdi, M. Zhou, D. Veysset, S. E. Kooi, Y. Jiao, M.-S. Hsiao, J. Streit,

R. A. Vaia and E. L. Thomas, *Materials Today*, 2018, **21**, 817–824.

7 E. P. Chan, W. Xie, S. V. Orski, J.-H. Lee and C. L. Soles, *ACS Macro Lett.*, 2019, **8**, 806–811.

8 J. Hyon, M. Gonzales, J. K. Streit, O. Fried, O. Lawal, Y. Jiao, L. F. Drummy, E. L. Thomas and R. A. Vaia, *ACS Nano*, 2021, **15**, 2439–2446.

9 L. Monnerie, J. L. Halary and H.-H. Kausch, *Intrinsic Molecular Mobility and Toughness of Polymers I*, Springer, Berlin, Heidelberg, 2005, pp. 215–372.

10 D. Shah, P. Maiti, D. D. Jiang, C. A. Batt and E. P. Giannelis, *Advanced Materials*, 2005, **17**, 525–528.

11 D. Maillard, S. K. Kumar, B. Fragneaud, J. W. Kysar, A. Rungta, B. C. Benicewicz, H. Deng, L. C. Brinson and J. F. Douglas, *Nano Lett.*, 2012, **12**, 3909–3914.

12 S. K. Kumar, B. C. Benicewicz, R. A. Vaia and K. I. Winey, *Macromolecules*, 2017, **50**, 714–731.

13 S. K. Kumar, N. Jouault, B. Benicewicz and T. Neely, *Macromolecules*, 2013, **46**, 3199–3214.

14 J. Choi, C. M. Hui, J. Pietrasik, H. Dong, K. Matyjaszewski and M. R. Bockstaller, *Soft Matter*, 2012, **8**, 4072–4082.

15 C. A. Grabowski, H. Koerner, J. S. Meth, A. Dang, C. M. Hui, K. Matyjaszewski, M. R. Bockstaller, M. F. Durstock and R. A. Vaia, *ACS Appl. Mater. Interfaces*, 2014, **6**, 21500–21509.

16 C. R. Bilchak, E. Buenning, M. Asai, K. Zhang, C. J. Durning, S. K. Kumar, Y. Huang, B. C. Benicewicz, D. W. Gidley, S. Cheng, A. P. Sokolov, M. Minelli and F. Doghieri, *Macromolecules*, 2017, **50**, 7111–7120.

17 J. Midya, M. Rubinstein, S. K. Kumar and A. Nikoubashman, *ACS Nano*, 2020, **14**, 15505–15516.

18 W. R. Lenart and M. J. A. Hore, *Nano-Structures & Nano-Objects*, 2018, **16**, 428–440.

19 M. Jhalaria, E. Buenning, Y. Huang, M. Tyagi, R. Zorn, M. Zamponi, V. García-Sakai, J. Jestin, B. Benicewicz and S. Kumar, *Phys. Rev. Lett.*, 2019, **123**, 158003.

20 J. G. Ethier, L. F. Drummy, R. A. Vaia and L. M. Hall, *ACS Nano*, 2019, **13**, 12816–12829.

21 J. M. Kubiak and R. J. Macfarlane, *Advanced Functional Materials*, 2019, **29**, 1905168.

22 J. Lee, Z. Wang, J. Zhang, J. Yan, T. Deng, Y. Zhao, K. Matyjaszewski and M. R. Bockstaller, *Macromolecules*, 2020, **53**, 1502–1513.

23 S. H. Chen, A. J. Souna, C. L. Soles, S. J. Stranick and E. P. Chan, *Soft Matter*, 2020, **16**, 3886–3890.

24 C. R. Bilchak, M. Jhalaria, Y. Huang, Z. Abbas, J. Midya, F. M. Benedetti, D. Parisi, W. Egger, M. Dickmann, M. Minelli, F. Doghieri, A. Nikoubashman, C. J. Durning, D. Vlassopoulos, J. Jestin, Z. P. Smith, B. C. Benicewicz, M. Rubinstein, L. Leibler and S. K. Kumar, *ACS Nano*, 2020, **14**, 17174–17183.

25 A. L. Bowman, E. P. Chan, W. B. Lawrimore and J. K. Newman, *Nano Lett.*, 2021, **21**, 5991–5997.

26 M. Rubinstein and R. H. Colby, *Polymer Physics*, Oxford University Press, USA, 1st edn, 2003.

27 C. L. Soles, A. B. Burns, K. Ito, E. Chan, J. Liu, A. F. Yee and M. S. Tyagi, *Macromolecules*, 2020, **53**, 6672–6681.

28 C. L. Soles, A. B. Burns, K. Ito, E. P. Chan, J. F. Douglas, J. Wu, A. F. Yee, Y.-T. Shih, L. Huang, R. M. Dimeo and M. Tyagi, *Macromolecules*, 2021, **54**, 2518–2528.

29 D. Parisi, E. Buenning, N. Kalafatakis, L. Gury, B. C. Benicewicz, M. Gauthier, M. Cloitre, M. Rubinstein, S. K. Kumar and D. Vlassopoulos, *ACS Nano*, 2021, **15**, 16697–16708.